Removal of antimonate and antimonite from water by schwertmannite granules

Yonghuan Li[a], Dinesh Mohan[b], Charles U. Pittman Jr.[c], Yong Sik Ok[d], Xiaomin Dou[a,]*

[a]*Department of Environmental Science and Engineering, Beijing Forestry University, P.O. Box 60, 100083 Beijing, P.R. China,*
emails: 18811798932@163.com (Y. Li), douxiaomin@bjfu.edu.cn (X. Dou)
[b]*School of Environmental Sciences, Jawaharlal Nehru University, New Delhi 110067, India, email: dm_1967@hotmail.com*
[c]*Department of Chemistry, Mississippi State University, Mississippi State, Mississippi 39762, USA,*
email: CPittman@chemistry.msstate.edu
[d]*Korea Biochar Research Center and Department of Biological Environment, Kangwon National University, Chuncheon 200-701,*
Korea, email: soilok@kangwon.ac.kr

ABSTRACT

In order to overcome the drawbacks of small particle-sized adsorbents, schwertmannite powder was fabricated into granules in the present study. These granules were evaluated for Sb(III) and Sb(V) removal from water and intraparticle mass transfer resistance of Sb(III) and Sb(V) onto the porous adsorbent was modeled. Schwertmannite granules (SG) exhibited capacities of 32.9 mg/g for Sb(III) and 23.2 mg/g for Sb(V), respectively, which are superior to many reported granular adsorbents and even powder adsorbents. Mass transfer was separately modeled using the pore volume diffusion model and surface diffusion model. The film diffusion coefficients, k_L, range from 1.09×10^{-5} to 3.08×10^{-5} cm/s. The pore diffusion coefficients, D_{ep}, range from 6.20×10^{-5} to 10.85×10^{-5} cm^2/s, and the surface diffusion coefficients, D_s, range from 1.12×10^{-9} to 3.57×10^{-9} cm^2/s. The concentration decay datasets were successfully fitted with these best obtained parameters. Sb(III) was effectively removed over a wide pH range, while the removal of Sb(V) was pH dependent and could be enhanced by lowering solution pH. Sb(III)-loaded SG was regenerated with 91.2% re-adsorption capacity retained after five cycles when using 0.6% NaOH as the stripping solution. The desorption of Sb(V) was not as successful as Sb(III). Before breakthrough (5 μg/L) occurred, 1,690 and 712 bed volumes (BVs) of Sb(III), and 769 and 347 BVs of Sb(V) were treated when operating at space velocity values of 2 and 6 h^{-1}, respectively. Considering the low cost and the granular form of schwertmannite, the adsorbent is a promising modestly priced adsorbent and can be easily used in packed bed or filter units for practical application.

Keywords: Antimonite; Antimonate; Granular adsorbent; Schwertmannite; Mass transfer; Model

*Corresponding author.

1. Introduction

Antimony (Sb) occurrence and contamination in aquatic and soil systems have raised extensive concern since recent findings elucidated its health effects [1]. Antimony is ubiquitous in the environment as a result of natural processes and human activities. Typical concentrations of total dissolved antimony are usually below 1.0 μg/L in non-polluted waters [1]. Elevated Sb concentrations can be observed in geothermal springs, Sb mining and smelting areas, shooting ranges, and municipal waste incineration plants [1–3]. Human exposures to antimony vary from inhalation in Sb-processing working areas, intake from contaminated diets and groundwater, and release from Sb-containing food packages (plastic, ceramic, drinking cup, etc.) [4]. Antimony and its compounds are considered to be priority pollutants by the USEPA and the EU. Rigorous guidelines or regulation limits for antimony in water have been set by international agencies and many countries. These limits include: WHO, 20 μg/L; USEPA, 6 μg/L; HC (Health Canada), Canada, 6 μg/L; EU, 5 μg/L; Ministry of Health (MOH), China, 5 μg/L, etc. [5–8].

Sb(V) and Sb(III) are the most frequently observed species in natural aquatic environments. $Sb(OH)_6^-$ is the predominant species of Sb in oxygenated aqueous systems and $Sb(OH)_3$ in anoxic water and pore water [1]. Several studies have concluded that iron and aluminum (oxy)hydroxides and oxides, such as schwertmannite, goethite, ferrihydrite, boehmite, and gibbsite appear to be excellent adsorbents for antimony mitigation from water [9–13]. Recently, schwertmannite has attracted substantial interest for hazardous anion and heavy metal removal from water, and it is an effective scavenger for antimony, arsenic, fluoride, Cu^{2+}, etc. [12–15]. Schwertmannite is a poorly crystalline Fe(III)-oxyhydroxy sulfate mineral with a variable composition, typically represented as $Fe_8O_8(OH)_{8-2x}(SO_4)_x$ (where x falls within 1–1.75), which occurs naturally in acid mine drainage. It can be chemically synthesized [16,17] or biosynthesized [18,19].

Freshly synthesized schwertmannite consists of small particle-sized colloids or precipitates [14,15]. This is a drawback for engineering pollution mitigation systems. Small particles cause large pressure drops in packed plug flow units. It can raise turbidity and colloid levels in effluent. The operation and maintenance of such small particle units would be difficult. The complete separation from effluent, recycle in continuous flow stirred-tank reactors (CSTRs), or satisfactory flow through packed columns require converting schwertmannite into granules to be used effectively in practice.

We previously reported several granulation methods including vibration-dropping, spray coating, extrusion, and drum granulation, which allowed the resulting granules to be used for AsO_4^{3-} removal [16,20]. Here, a schwertmannite granule (SG) adsorbent was made and evaluated for Sb(III) and Sb(V) removal. Since granular schwertmannite is porous, mass transfer resistance is involved in its use in batch and continuous operations. Thus, investigation of the mass transfer of adsorbate onto SG would be valuable for adsorbent comparison and adsorption unit design. The mass transfer behavior of Sb(III) and Sb(V) within SG was simulated using both the pore volume diffusion model (PVDM) [21] and the surface diffusion model (SDM) [22], both of which are introduced in detail in the Materials and methods section.

In the present study, SG was prepared and then evaluated in both batch and column tests. The removal efficiency was evaluated vs. contact time, initial concentration, and solution pH. The mass transfer process was modeled using both the PVDM [21] model and the SDM model [22]. The film diffusion coefficients (k_L), pore diffusion coefficients (D_{ep}), and surface diffusion coefficients (D_s) were numerically determined. The overall aims of this study were (1) to assess the capability of SG to remove Sb(III) and Sb(V) from water and (2) to demonstrate the mass transfer mechanisms of Sb(III) and Sb(V) onto the granular adsorbent.

2. Materials and methods

2.1. Materials

All chemicals were analytical grade reagents. The Sb(III) and Sb(V) stock solutions were prepared with deionized water using antimony potassium tartrate and potassium pyroantimonate, respectively. Solutions containing Sb(III)/Sb(V) were freshly prepared by diluting the stock solution with distilled water.

2.2. Adsorbent preparation and characterization

Schwertmannite powder was prepared following a modified procedure from Cornell and Schwertmann [16,17], using $FeCl_3$ and Na_2SO_4 as reactants in a $4\ m^3$ stirred-tank reactor. The deionized water ($2\ m^3$) was fed into the reactor and heated to 60°C first. Then, the raw reactants were quickly added to obtain concentrations of 0.02 mol/L Fe^{3+} and 0.01 mol/L SO_4^{2-}. The solution was vigorously stirred and maintained at 60°C for 12 min. Then the mixture was cooled to room temperature. The suspension was washed five times using deionized water and dried in a spray-drying

tower. The schwertmannite powder has a BET surface area of 206.1 m^2/g. Then SGs with an irregular shape were fabricated on an oscillating granulator using a drum granulation procedure, as described in our previous report [16]. The final products were oven-dried at 60℃ for 24 h and stored in a desiccator for further use. The granules had an average diameter of 1.3 mm. The surface area, bulk density, void fraction, and pore tortuosity were SA = 199.43 m^2/g, ρ_P = 0.33 g/cm^3, ε_P = 0.359, and τ = 1.824, respectively.

2.3. Batch adsorption experiments

Isotherm experiments on SG were carried out at 25 ± 1℃. Initial Sb(III) or Sb(V) concentrations from 0 to 70.57 mg/L, respectively, were used with an adsorbent dose of 1 g/L at a pH of 7.0 ± 0.2. After shaking for 48 h, the residual Sb(III) or Sb(V) was analyzed in the filtrate, which had been separated using a 0.45-μm membrane.

A Sb(III)/Sb(V) stock solution and deionized water were added into each of a series of 2,000-ml glass conical flasks to achieve an initial Sb(III) concentration of ca. 22 mg/L or Sb(V) concentration of ca. 23 mg/L, with a total volume of 1,000 ml. Then, the granular adsorbents were added at a dose of 0.5, 1, 2, and 4 g/L, respectively, for either the Sb(III) or Sb(V) solution. The pH of these mixtures was adjusted and maintained at 7.0 ± 0.2 throughout the experiment. These mixtures were shaken at 120 rpm and maintained at 25 ± 1℃. Approximately 3-ml aliquots were taken from each suspension at predetermined intervals. These samples were immediately filtered through a 0.45-μm membrane, and then the residual Sb in solution was analyzed.

The effect of solution pH on the Sb removal was studied in 250-ml glass bottles containing 100 ml of Sb solution with 8.98 mg/L of Sb(III) or 9.49 mg/L of Sb(V) and a SG dose of 1 g/L. The pH was adjusted and maintained at a specified value in the range from 3.5 to 9.0. Temperature was maintained at 25 ± 1℃. A shaking time of 24 h was maintained, then the suspension was filtered through a 0.45-μm membrane, and the residual Sb(III) or Sb(V) was analyzed.

2.4. Regeneration and reuse experiments

SG adsorbent regeneration studies were carried out in a batch mode. Sb(III) or Sb(V) was first adsorbed from 100 ml solutions with respective initial concentrations of 9.30 mg/L, a granular adsorbent dose of 1 g/L, and pH of 7.0 ± 0.2. After a 10-h adsorption period, the granular adsorbents were then collected by

filtration and placed into 100 mL of pH 5 deionized water (adjusted by HCl) for 4 h to neutralize residual alkali in the pores. The SG was air-dried for further regeneration experiments. The regeneration experiments were performed by shaking the Sb-loaded adsorbent in 100 mL NaOH solutions of different concentrations for a period of 10 h at 25 ± 1℃. Then, the regenerated SGs were reused for Sb(III) or Sb(V) adsorption applying the same conditions as the first adsorption step. The regeneration–reuse experiments were repeated for five times.

2.5. Column experiments

Column studies on the SGs were performed in perspex columns with an inner diameter of 2.0 cm and a length of 40 cm. The height of the packed SG bed was 20 cm and the volume was 62.8 ml. Sb(III) (200 μg/L) or Sb(V) (200 μg/L) spiked deionized water, respectively, was used as the influent. The SG columns were operated at space velocity (SV) values of 2 and 6 h^{-1}, respectively. SV refers to the quotient of the entering volumetric flow rate of the reactants divided by the reactor volume (or the adsorption bed volume). SV indicates how many reactor volumes of feed can be treated in a unit time. The corresponding empty bed contact times (EBCT) were 30 and 10 min, and the superficial liquid velocity (SLV) were 0.4 and 1.2 m/h, respectively. The effluent was collected at regular intervals and the Sb concentrations were measured. A breakthrough value of 20 μg/L was set for the column study.

2.6. Diffusion model

Three well-known simultaneous steps, including external mass transfer (also called film diffusion), intraparticle diffusion, and adsorption on active surface sites, generally account for the overall adsorption rate by porous adsorbents [21,23]. During batch adsorption, intraparticle diffusion could occur as pore volume diffusion, surface diffusion, or both [24]. A general diffusion model (Eqs. (1)–(6)) summarizing the three steps was proposed by Leyva-Ramos [23,25]. This model has been successfully used in pharmaceuticals personal care products (PPCPs), phenol, and fluoride adsorption on porous materials [21,22,24,26]:

$$V\frac{dC_A}{dt} = -mSk_L(C_A - C_{A,r}|_{r=R_p}) \tag{1}$$

$$t = 0, \quad C_A = C_{A0} \tag{2}$$

$$\varepsilon_p \frac{\partial C_{A,r}}{\partial t} + \rho_p \frac{\partial q}{\partial t} = \frac{1}{r^2} \frac{\partial}{\partial r} \left[r^2 \left(D_{ep} \frac{\partial C_{A,r}}{\partial r} + D_s \rho_p \frac{\partial q}{\partial r} \right) \right] \quad (3)$$

$$C_{A,r} = 0, \quad t = 0, \quad 0 \leq r \leq R_p \quad (4)$$

$$\frac{\partial C_{A,r}}{\partial r} \Big|_{r=0} = 0 \quad (5)$$

$$D_{ep} \frac{\partial C_{A,r}}{\partial r} \Big|_{r=R_p} + D_s \rho_p \frac{\partial q}{\partial r} \Big|_{r=R_p} = k_L (C_A - C_{A,r} |_{r=R_p}) \quad (6)$$

where Eq. (1) is the film diffusion equation and Eq. (3) is the pore diffusion equation. Eqs. (2) and (4) are initial conditions for C_A and $C_{A,r}$, and Eqs. (5) and (6) are boundary conditions for Eq. (3). The mass transport parameters of the general diffusional model are the external transfer coefficient (k_L), surface diffusion coefficient (D_s), and effective diffusion coefficient in the pore volume (D_{ep}). The general model may be simplified as the PVDM or as the SDM, respectively, by assuming the pore volume diffusion is the only intraparticle diffusion mechanism ($D_{ep} \neq 0$, $D_s = 0$), or considering that surface diffusion contributes exclusively to intraparticle diffusion ($D_{ep} = 0$, $D_s \neq 0$) [23,27].

The rate of adsorption on active sites is assumed to be instantaneous, once the adsorbate reaches the active site. The amount of adsorbed adsorbate, q, can be related to the adsorbate concentration in the pore volume, $C_{A,r}$, by adsorption isotherm equations, such as the Freundlich [25], Langmuir [24], or Radke–Prausnitz [28] isotherms.

The external mass transfer coefficient, k_L, was estimated using the method proposed by Furusawa and Smith [29]. This method is based on Eq. (1), which was evaluated at the initial conditions $t = 0$, when the adsorbate concentration on the porous adsorbent surface is close to zero, $C_{A,r} \approx 0$. Substituting these conditions in Eq. (1) gives:

$$\frac{d(C_A/C_{A0})}{dt} = -k_L \frac{V}{mS} \quad (7)$$

The term on the right was calculated using the first two points at $t = 0$ min and $t = 10$ min of the kinetics data-sets.

The SGs were treated here as spheres for simplification. The mass transfer of Sb(III) and Sb(V) into SG was modeled using the approach described above. The coupled partial and ordinary differential equations were numerically solved using the program PDE2D v9.4 free version with the Lahey Fortran compiler LF90 v4.5 [30].

2.7. Analytical methods

The residual Sb(III)/Sb(V) concentrations were analyzed by a hydride generation-atom fluorescence spectrometer (HG-AFS, AF-610D2, Beijing Rayleigh Analytic Instrument Corporation, China) using a published method [31].

3. Results and discussion

3.1. Adsorption isotherm of Sb(III) and Sb(V) on SG

The adsorption capacity at a given condition is a basic and critical parameter for comparing and screening adsorbents, designing adsorption units, and optimizing operation conditions. Higher capacity means longer service time and lower costs involved for adsorbent replacement, regeneration, and other maintenance operations.

The Sb(III) and Sb(V) adsorption isotherms on SG are presented in Fig. 1. The equilibrium data were fitted to three isotherm equations, including the Langmuir [32], Freundlich [33], and Radke–Prausnitz [28] isotherm models. The corresponding model parameters are summarized in Table 1. In general, slightly higher correlation coefficients and smaller root-mean-square errors (RMSE) for q (Eq. (8)) were observed using the Radke–Prausnitz isotherm than using the Langmuir isotherm or the Freundlich isotherm (Table 1) for both Sb(III) and Sb(V) adsorption. This is as expected since the Radke–Prausnitz isotherm is a three-parameter model, which fitted the experimental data reasonably well, yielding
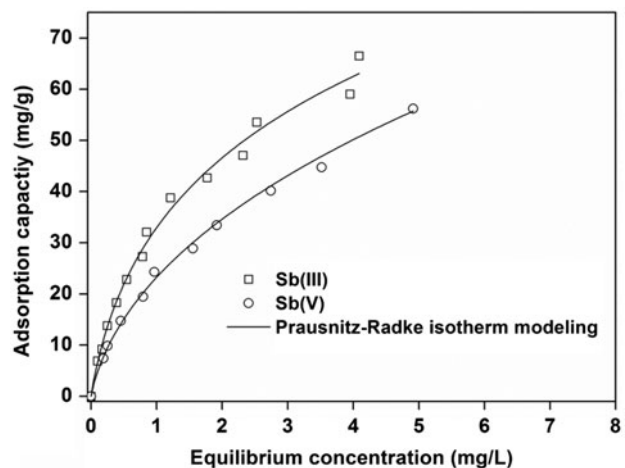
Fig. 1. The Sb(III) and Sb(V) adsorption isotherms on SGs. Initial Sb(III) or Sb(V) concentrations, 0–70.57 mg/L; adsorbent dose, 1 g/L; shaking time, 48 h; pH, 7.0 ± 0.2, temperature, 25 ± 1°C.

Table 1
Adsorption isotherm parameters for Sb(III) and Sb(V) adsorption on the SGs

| Equations | Parameters | Values | |
		Sb(III)	Sb(V)
Langmuir $q_e = \frac{q_{max} b C_e}{1 + b C_e}$	q_{max} (mg/g)	84.03	78.60
	b (L/mg)	0.668	0.416
	R_L^2	0.988	0.988
	RMSE	2.19	1.93
Freundlich $q_e = k C_e^{1/n}$	k	31.37	22.69
	n	1.933	1.771
	R_F^2	0.985	0.996
	RMSE	2.46	0.94
Prausnitz–Radke $q_e = \frac{a C_e}{1 + b C_e^\beta}$	a	84.77	77.20
	b	1.574	2.321
	β	0.745	0.576
	R_{PR}^2	0.990	0.997
	RMSE	1.83	0.86

determination coefficients (R^2) above 0.990 and the RMSE value less than 1.83.

$$RMSE_q = \sqrt{\frac{\sum_{i=1}^{n} (q_{exp} - q_{pred})^2}{n}} \quad (8)$$

SG show a higher uptake capacity for Sb(OH)$_3$ (84.03 mg/g) than Sb(OH)$_6$ (78.60 mg/g) at pH 7.0. A similar phenomenon was observed previously for Sb(III) and Sb(V) adsorption on goethite, akaganéite, and hematite at pH 4.0, 7.0, and 9.0 [9]. Mason et al. [34] indicated that hydrated hematite has a larger favorable adsorption energy and higher reactivity toward Sb(III) than Sb(V) using density functional theory (DFT) modeling. This provided a clue to understand the binding behavior difference of Sb(III) and Sb(V) on SG. Differences could also be attributed to the possible exchange with the sulfate groups present in the schwertmannite particles. A study conducted by Burton et al. [15] on As(III) and As(V) binding on schwertmannite points out the different anion exchange ratio produced for these two ions. A similar behavior could be expected for Sb(III) and Sb(V) on SG.

It is worthwhile to compare the Sb(III) and Sb(V) adsorption capacities of SG with other granular adsorbents reported in the literature. Considering the Sb concentration ranges found in polluted areas [35], these adsorbents were compared under a fixed equilibrium concentration of 1 mg/L Sb(III) or Sb(V) at pH 7.0 (Table 2). SG exhibited a better performance than

many reported adsorbents. There are three reasons for this result. First, schwertmannite shows good Sb(V) and Sb(III) removal [9]. Second, we used a drum granulation procedure, which can fabricate better granules (with a BET surface area of 199.4 m^2/g) than the extrusion granulation procedure (189.3 m^2/g), spray-coating (32.5 m^2/g), or other coating granulation procedures [16]. Third, both complexation to the surface hydroxyl groups and anion exchange could contribute to adsorption. This leads to an additional adsorption compared with other iron oxides.

3.2. Experimental kinetic data for Sb(III) and Sb(V) adsorption on SG

Adsorption kinetic parameters are critical for designing adsorption units and optimizing operational conditions. First, kinetics data is used to make decisions about the adsorbent type and which specific adsorbent will be selected for use. Second, the kinetic properties control the required contact time of a batch reactor or the cycle time of a fixed bed adsorption process. Third, modeling kinetics using adsorption diffusion models (e.g. film diffusion model (FDM), PVDM, SDM or their combinations) can reveal more information on mass transfer across the liquid film or within particle. This helps to understand the removal process within granular adsorbents.

Figs. 2–5 show the experimental concentration decay curves of Sb(III) and Sb(V) sorption from water onto SG at various adsorbent dosages. Equilibrium time was gradually shortened when the adsorbent dosage increased from 0.5 to 4 g/L. The equilibrium was reached within 4 h with a dosage of 4 g/L for both Sb(III) and Sb(V) adsorption, and most sorption (>95.7%) took place within this period. After 4 h, there was a negligible increase in adsorption rate and the residual Sb(III) and Sb(V) concentrations remained almost unchanged.

3.2.1. Calculation of external mass transport parameters, k_L

The external mass transfer coefficient (k_L) represents the resistance of external mass transfer or the so-called film resistance across the liquid film in the outer surface of the adsorbents. It was calculated using Eq. (7). The estimated k_L values are given in Table 3. They ranged from 1.09×10^{-3} to 3.08×10^{-3} cm/s, and decreased with increasing SG dosages for Sb(III) adsorption. This drop in k_L resulted from a lower concentration driving force per mass of

Table 2
A performance comparison between the SGs and various reported adsorbents for Sb(III) and Sb(V) removal from water

Adsorbent	Adsorbates	Adsorbent forms	Dose (g/L)	Temperature (℃)	pH	Equilibrium Time (h)	Capacity (mg/g)	Refs.
Granular schwertmannite	Sb(III)	1.0–1.6 mm	1	25 ± 1	7.0 ± 0.2	48	32.9 (Radke–Prausnitz isotherm)	Present study
PVA-Fe^0	Sb(III)	Granules, 2.04 ± 0.98 mm	2	25 ± 1	7.0 ± 0.2	48	2.6 (Langmuir isotherm)	[36]
Hematite modified nano-magnetite	Sb(III)	Fine powder	0.1	25	4.1	36	23.9 (Freundlich isotherm)	[37]
Commercial nano-magnetite	Sb(III)	Fine powder	0.1	25	4.1	36	10.3 (Freundlich isotherm)	[37]
Coated quartz sand	Sb(III)	0.6–0.8 mm	20	25 ± 0.5	7.0 ± 0.1	24	0.9 (Langmuir isotherm)	[38]
Graphene-schwertmannite composites	Sb(III)	Fine powder	0.3	25 ± 1	7.0 ± 0.2	24	54.7 (Langmuir isotherm)	[12]
Goethite (α-FeOOH)	Sb(III)	Fine powder	0.7	25	3.9 ± 0.7	24	1.9 (Langmuir isotherm)	[39]
Granular schwertmannite	Sb(V)	1.0–1.6 mm	1	25 ± 1	7.0 ± 0.2	48	23.2 (Radke–Prausnitz isotherm)	Present study
PVA–Fe^0	Sb(V)	Granules, 2.04 ± 0.98 mm	2	25 ± 1	7.0 ± 0.2	48	0.4 (Langmuir isotherm)	[36]
Iron-zirconium bimetal oxide	Sb(V)	Fine powder	0.2	25 ± 1	7.0 ± 0.2	24	46.9 (Langmuir isotherm)	[40]
Commercial akaganeite, GEH	Sb(V)	<100 μm	2	Room temperature	7.0	24	27.5 (Langmuir isotherm)	[41]
Synthetic akaganeite	Sb(V)	Fine powder	2	Room temperature	7.0	24	41.8 (Langmuir isotherm)	[41]
HFO-polymeric anion exchanger	Sb(V)	Spherical shape, 0.6–0.7 mm	0.5	25	6	24	17.0 (Langmuir isotherm)	[42]
HFO-calcite	Sb(V)	Irregular shape, 0.45–0.9 mm	0.5	25	6	24	7.3 (Langmuir isotherm)	[42]

Note: The performances were compared at an equilibrium concentration of 1 mg/L and an adsorbent dose of 1 g/L at pH 7.0 ± 0.1.

adsorbent (($C_{A0} - C_A$)/g-adsorbent). The change in k_L values for Sb(V) adsorption was more complicated. k_L increased when the initial Sb(V) concentration was raised from 23.63 to 26.37 mg/L accompanied with an adsorbent dosage increase from 0.5 to 2.0 g/L. Then k_L drops at a 4 g/L adsorbent dose. These changes were due to the increased driving force per mass adsorbent (($C_{A0} - C_A$)/g-adsorbent) when initial Sb(V) concentrations were raised first, and then a drop in the driving force when the dose reached 4 g/L. The k_L values listed in Table 3 were put into in Eq. (6) and combined to resolve the intraparticle mass transfer parameters, D_{ep} or D_s. That means the k_L values are the basic parameter for further modeling and the film diffusion process was incorporated into the pore volume diffusion or SDM.

_3.2.2. D_{ep} determination using the PVDM_

The concentration decay data-sets were fitted using the PVDM as presented in Eqs. (1)–(6). According to the PVDM model, the intraparticle diffusion is exclusively due to pore volume diffusion. The mass transfer parameters of the PVDM model are k_L and D_{ep}. k_L was estimated with Eq. (7). D_{ep} was solved numerically by setting $D_s = 0$. The optimal value of D_{ep} was
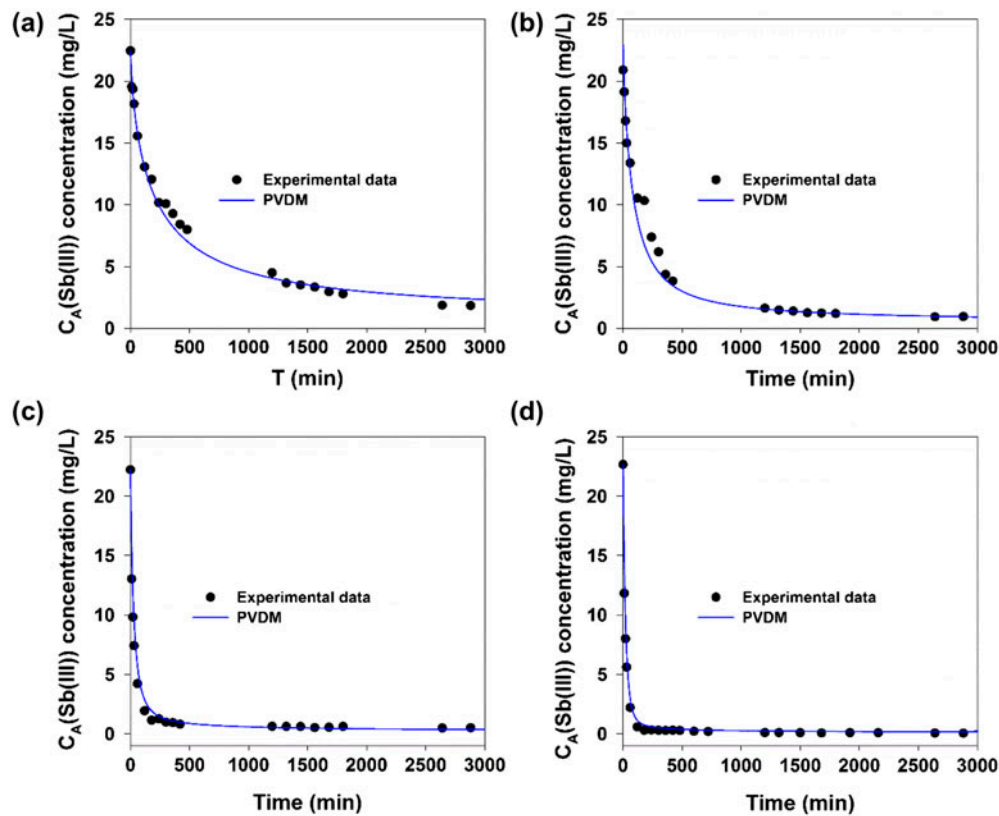
Fig. 2. PVDM modeling of Sb(III) adsorption on SGs with adsorbent doses of (a) 0.5 g/L, (b) 1 g/L, (c) 2 g/L and (d) 4 g/L, respectively. Initial Sb(III) concentrations, 22.21–22.93 mg/L; pH, 7.0 ± 0.2; shaking speed, 150 rpm; temperature, 25 ± 1°C.

Table 3
Experimental conditions and mass transfer coefficients for Sb(III) and Sb(V) adsorption on the SGs

Species	C_{A0} (mg/L)	m (g)	C_e (mg/L)	q_e (mg/g)	$k_L \times 10^3$ (cm/s)	$D_{ep} \times 10^6$ (cm^2/s)	$D_s \times 10^9$ (cm^2/s)
Sb(III)	22.45	0.5	1.84	41.22	3.08	6.20	2.33
	22.94	1.0	0.95	21.99	1.98	6.28	1.57
	22.21	2.0	0.49	10.86	1.67	8.98	1.53
	22.66	4.0	0.47	5.55	1.43	10.28	1.12
Sb(V)	23.63	0.5	2.30	42.66	1.09	10.85	3.57
	23.81	1.0	0.72	23.09	1.89	9.78	2.71
	26.37	2.0	0.33	13.02	2.16	7.01	1.88
	26.30	4.0	0.15	6.54	1.69	9.45	1.48

obtained by minimizing the RMSE values for C_A (Eq. (9)):

$$RMSE_{C_A} = \sqrt{\frac{\sum_{i=1}^{n} (C_{A,exp} - C_{A,pred})^2}{n}} \qquad (9)$$

The optimal value of D_{ep} and corresponding fitting parameters are summarized in Table 3. The fitting curves using the PVDM model with the best fitted D_{ep} values are presented in Figs. 2 and 3. The best fitting values of D_{ep} vary from 6.20×10^{-6} to 10.85×10^{-6} cm^2/s.
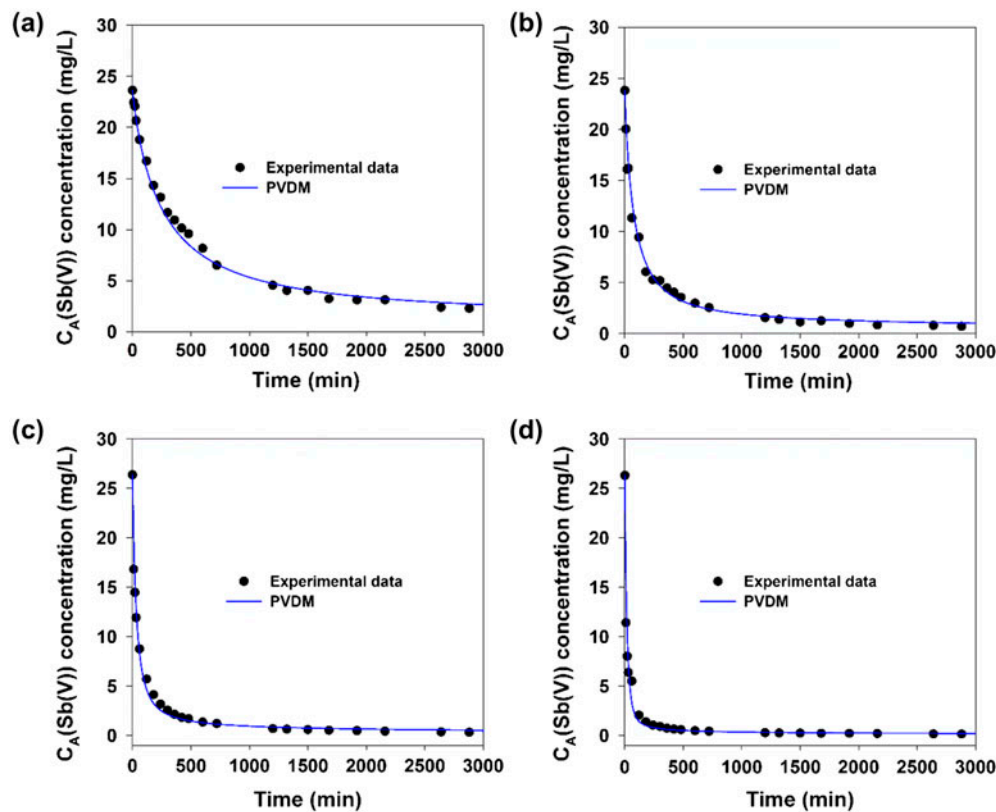
Fig. 3. PVDM modeling of Sb(V) adsorption on SGs with adsorbent doses of (a) 0.5 g/L, (b) 1 g/L, (c) 2 g/L and (d) 4 g/L, respectively. Initial Sb(V) concentrations, 23.62–26.37 mg/L; pH, 7.0 ± 0.2; shaking speed, 150 rpm; temperature, 25 ± 1°C.

3.2.3. D_s determination using the SDM

The concentration decay data-sets were separately fitted using the SDM model (Figs. 4 and 5). In the SDM model, the intraparticle diffusion is solely due to surface diffusion. The mass transfer parameters of the SDM model are k_L and D_s as described in Eqs. (1)–(6). Eq. (7) was used to estimate k_L. D_s was solved numerically with $D_{ep} = 0$ and the optimal value was obtained by minimizing the RMSE value (Eq. (9)). The fitting parameters obtained are summarized in Table 3. The fitting curves using the SDM model with the best fitted D_s values are presented in Figs. 4 and 5. The best fitting values of D_s range from 1.12×10^{-9} to 3.57×10^{-9} cm^2/s.

The effect of the mass of Sb(III) or Sb(V) adsorbed at equilibrium, q_e, on the surface diffusion coefficients, D_s, was analyzed, respectively (Fig. S1). D_s for both Sb (III) and Sb(V) adsorption increased with increasing amounts of q_e. Similar D_s changes were reported for phenol adsorption on organobentonite [24], dyes [43] and pentachlorophenol [44] adsorption on granular activated carbon. Mollah and Robinson [45] suggested a relationship between q_e and D_s as described in Eq. (10):

$$D_s = D_{s0} \ e^{\alpha q_e} \tag{10}$$

where D_{s0} (cm^2/s) is the effective surface diffusion coefficient at zero surface coverage and α (g/mg) is a constant in Eq. (10). The best fitted D_{s0} and α values were 1.11×10^{-8} cm^2/s and 0.018 g/mg for Sb(III) adsorption, and 1.47×10^{-8} cm^2/s and 0.021 g/mg for Sb(V) adsorption, respectively, corresponding to SG dosages of 0.5 to 4 g/L. The fitting curves with the obtained D_{sq} and α values are plotted in Fig. S1. The influence of q_e on D_s could be explained by the differences in solid-phase driving force at different q_e values. High q_e means high solid phase concentration and large amounts of adsorbates adsorbed on intraparticle surface sites. High-adsorption energy sites only account for small portions of these occupied surface sites. A greater number of adsorbates on low-adsorption energy sites could migrate on the surface from one site to another [24]. High q_e resulted in high
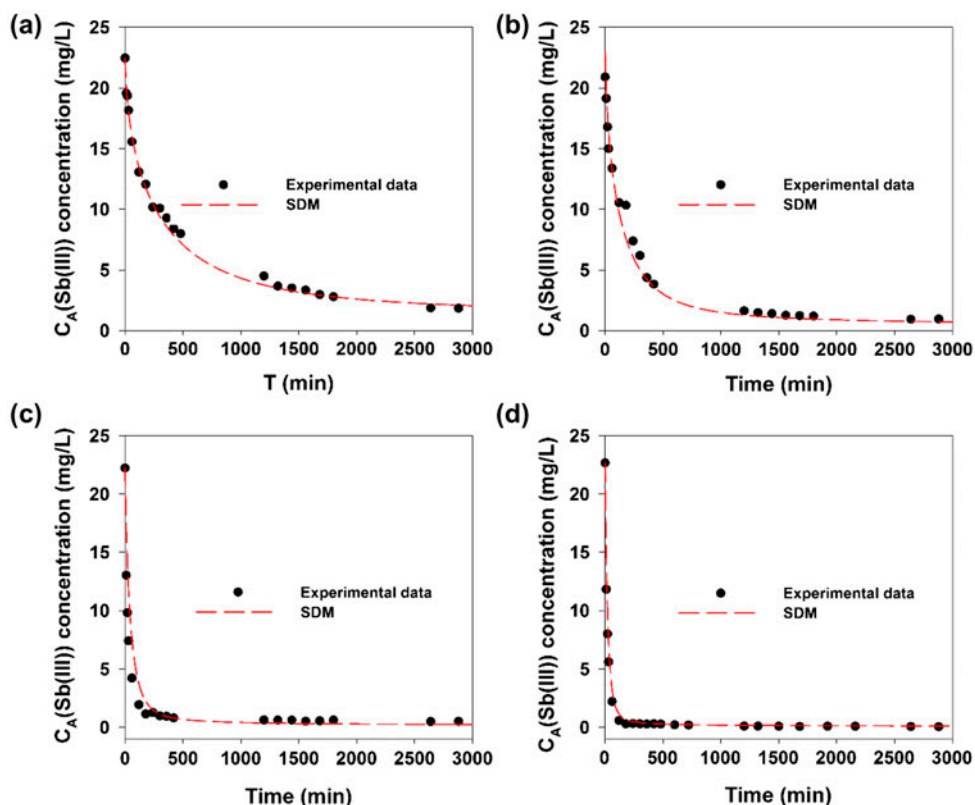
Fig. 4. SDM modeling of Sb(III) adsorption on SGs with adsorbent doses of (a) 0.5 g/L, (b) 1 g/L, (c) 2 g/L and (d) 4 g/L, respectively. Initial Sb(III) concentrations, 22.21–22.93 mg/L; pH, 7.0 ± 0.2; shaking speed, 150 rpm; temperature, 25 ± 1°C.

migration probabilities on intraparticle surfaces. Thus, enlarged values of D_s were observed with greater q_e values.

Since there are no reported molecular diffusion coefficient values (D_{AB}) for antimonite and antimonate in water, the theoretical pore volume diffusion coefficient could not be estimated using established equations for them. Thus, the relative contribution of pore volume diffusion or surface diffusion to overall intraparticle diffusion could not be evaluated. That means either pore volume diffusion mechanism or surface diffusion mechanism could not be excluded from the intraparticle diffusion of Sb(III)/Sb(V) on SG. The intraparticle diffusion in the present study could be reasonably represented using both the PVDM and SDM models with the obtained D_{ep} and D_s parameters.

3.3. Effect of pH on adsorption

Sb(III) and Sb(V) removals by SG vs. pH are shown in Fig. 6. Sb(III) was effectively removed over a wide pH range of 3.5–9.0. Sb(V) adsorption remained nearly constant in the pH 3.5–5.0 range and then dropped at pH above 5.0. The difference in Sb(III) and Sb(V) efficiency may occur due to electrostatic force differences existing between the sorbent surface and antimony oxyanions present in solution. $Sb(OH)_6^-$ is the dominate Sb(V) solution species existing over the pH range (4–10) examined [1]. The pHpzc of the active phase in granules is 5.1–7.2 [12,46]. Thus, lower pH (<pH 5.1) favors more sorbent surface protonation. At pH above 5.1, surface of oxides is increasingly deprotonated and negative charges increase on the surface that enhance electrostatic repulsions between the surface and negatively charged $Sb(OH)_6^-$. Neutral $Sb(OH)_3$ is the dominate Sb(III) species present over the pH range of 3–11 [1]. Thus, increasing negative charges on the surface don't repel neutral $Sb(OH)_3$ and its high removal capacity is maintained as pH increases. Improved Sb(III) vs. Sb(V) removal as pH is increased above 5.1, is likely due to reduced surface repulsion forces relative to those experienced by $Sb(OH)_6^-$ as pH increases, especially at high pH values.
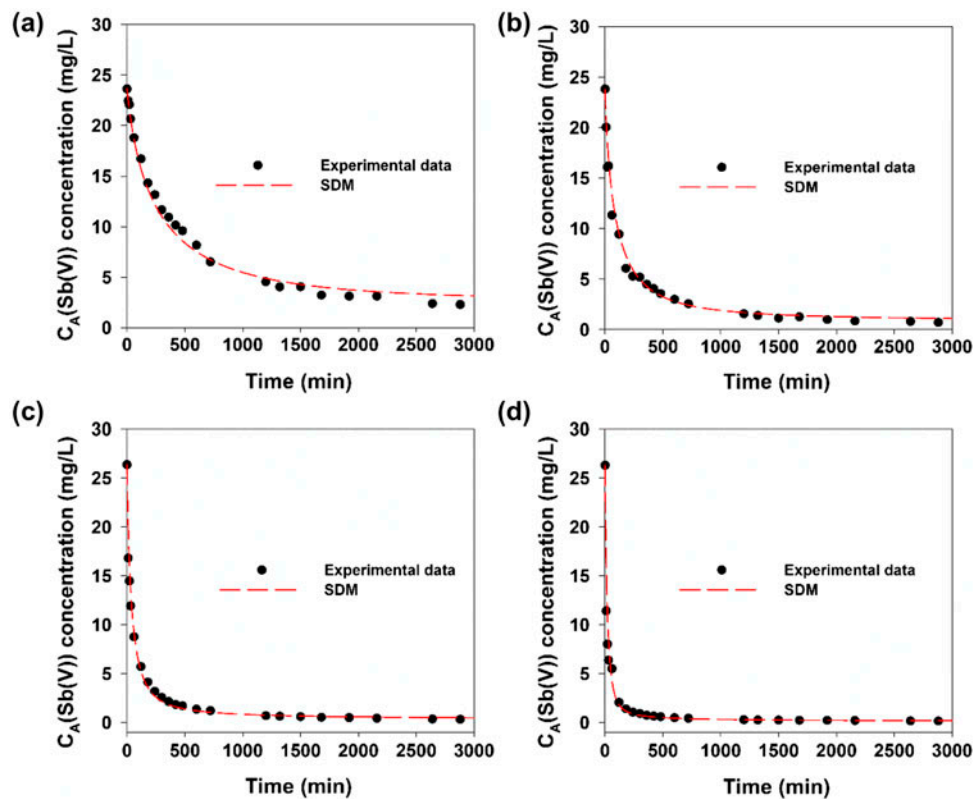
Fig. 5. SDM modeling of Sb(V) adsorption on SGs with adsorbent doses of (a) 0.5 g/L, (b) 1 g/L, (c) 2 g/L and (d) 4 g/L, respectively. Initial Sb(V) concentrations, 23.62–26.37 mg/L; pH, 7.0 ± 0.2; shaking speed, 150 rpm; temperature, 25 ± 1°C.
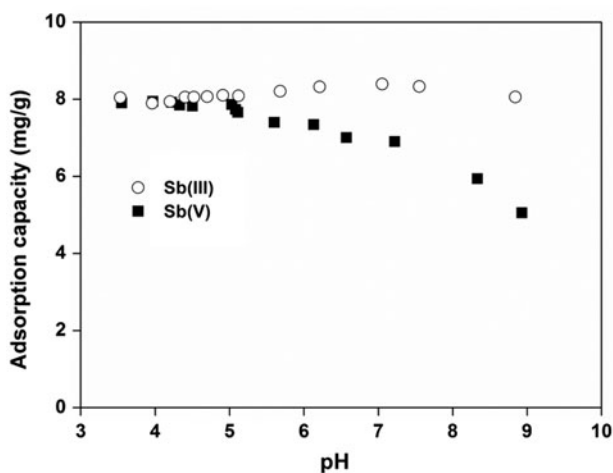
Fig. 6. Effect of solution pH on Sb(III) and Sb(V) adsorption by SGs. Initial Sb(III) concentration, 8.98 mg/L; initial Sb(V) concentration, 9.49 mg/L; adsorbent dose, 1 g/L; total solution volumes, 100 ml; pH range, 3.5–9.0; temperature, 25 ± 1°C, and shaking time, 24 h.

3.4. Batch regeneration and reuse

Regeneration and recycling of SG were evaluated using 2, 4, 6, and 8% aqueous NaOH stripping solutions over five regeneration cycles (Fig. 7). Although the extent of regeneration decreased upon repeated recycling, only slight drops in re-adsorption capability were observed for Sb(III) on SG. Using 6 and 8% NaOH stripping solutions led to slightly higher re-adsorption abilities vs. the use of 2 and 4% NaOH in the 4th and 5th cycles. More than 91.2% of the original Sb(III) adsorption capacity was maintained after five recycles using 6% NaOH. This concentration is considered as the best option. It gives lower NaOH consumption and less residual alkali within the regenerated granules in comparison to stripping with 8% NaOH. The Sb(V) re-adsorption capacities of SG dropped significantly after the 1st cycle in all cases. The re-adsorption ability gradually increased from 30.6 to 50.0% using increasing NaOH concentrations (2–8% in the 2nd cycle). However, more work is required to find an effective stripping method for Sb (V)-loaded SG. The unsatisfied re-adsorption capacity could be caused by residual alkali retention, pore and
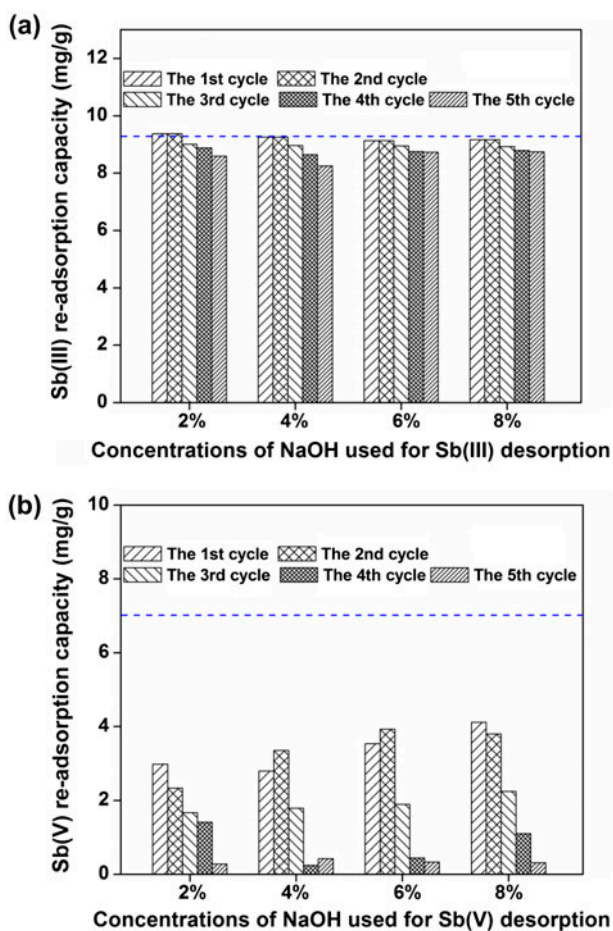
Fig. 7. Re-adsorption capabilities of SGs for (a) Sb(III) and (b) Sb(V) in 5 adsorption-regeneration cycles vs. the aqueous NaOH concentrations used for regeneration. Initial Sb (III) or Sb(V) concentrations, 9.30 mg/L; adsorbent dose, 1 g/L; pH, 7.0 ± 0.1, shaking time, 24 h; temperature, 25 ± 1℃.

surface properties changes, insufficient desorption and very subtle conversions of a mineral phase which was not strong enough to be identified by XRD (Fig. S2). On the other hand, another possible reason for the differences observed after use is how sulfate ions behave in this mineral. Increasing the pH may release a fraction of sulfate ions upon facial exchange with the Sb ions. Sulfate ions may not be re-adsorb during the regeneration process conducted here, therefore changing schwertmannite reactivity. According to USEPA's suggested solutions [47], the effluent from the regeneration stage could be safely discharged into publicly owned treatment works (POTW) after antimony removal and pH adjustment. In a similar way, Sb(III)

or Sb(V) was readily precipitated using FeCl₃, and then discharged into POTW. A coagulation experiment (Table S1) showed that 5 mg/L Sb(III) or Sb(V) was readily be precipitated by 40 and 60 mg/L FeCl₃, respectively, after adjusting pH to 8.0. The residual Sb (III) and Sb(V) concentrations were lower than 1.0 mg/L. Then the precipitate could be separated and finally disposed. The residual brine (pH 6–9) could be discharged into POTW. Accordingly, a discharge permit must be filed with the local agency for this discharge.

3.5. Column tests using Sb(III) or Sb(V)-spiked water

Column or fixed bed dynamics represent among the most important and necessary data for adsorber or adsorption unit design. The lifespans before breakthrough that occurred at various operational conditions can be used for scaling up adsorber units. In the present study, columns were operated with an influent Sb(III) or Sb(V) concentration of 200 μg/L (Fig. 8). Before the Sb concentration in the effluent reached the 5 μg/L regulation limit (MOH, China), 1,690 and 712 bed volumes (BVs) of Sb(III), and 769 and 347 BVs of Sb(V), operated at SV values of 2 and 6 h^{-1}, respectively, were treated. More than 2,700 and 1,500 BVs of Sb(III), and 1,790 and 650 BVs of Sb(V) could be treated before breakthrough when operated at these same SV values, respectively, if the WHO guideline (20 μg/L, the breakthrough value) was applied. This confirmed that this granular adsorbent has a good performance in the continuous treatment of Sb(III) or Sb(V), and the adsorbent has a great potential as a practical adsorbent candidate. The parameters obtained in this work could be used as the basic parameters in further scaling up design. In addition, a mass balance calculation indicated that the concentrations of total loaded adsorbates onto packed SG column were about 1.01 and 0.44 mg/g of Sb(III), and 0.57 and 0.24 mg/g of Sb(V), respectively, at SV values of 2 and 6 h^{-1}. The cumulative capacities of the column tests were far lower than the values of 11.50 mg-Sb(III)/g-SG (pH 7.0) and 8.05 mg-Sb (V)/g-SG (pH 7.0), respectively, calculated from the Radke–Prausnitz isotherm at an equilibrium concentration of 200 μg/L. Such phenomena has been commonly observed and reported in other studies [48]. These lower cumulative capacities were attributed to the low Sb(III) and Sb(V) concentration, short contact time, and mass transfer resistances within the column.
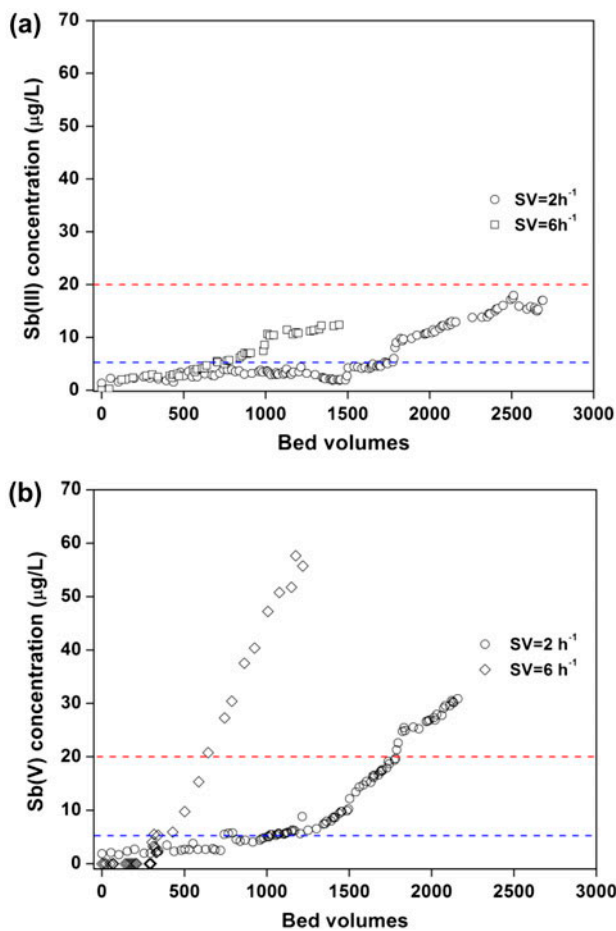
Fig. 8. Breakthrough curves from column experiments during Sb(III) and Sb(V) adsorption on SGs. Initial Sb(III) or Sb(V) concentration = 200 μg/L; influent pH, 7.0 ± 0.2, specific velocity (SV), 2 and 6 h^{-1}, respectively; SLV, 0.4 and 1.2 m/h, respectively.

4. Conclusions

SG exhibits a Sb(III) capacity of 32.9 mg/g and a Sb(V) capacity of 23.2 mg/g, with an equilibrium concentration of 1 mg/L and an adsorbent dose of 1 g/L at pH 7.0 ± 0.1. This performance is superior to many reported granular adsorbents. Sb(III) and Sb(V) sorption kinetics data-sets were successfully modeled using the PVDM and SDM, respectively. The film diffusion coefficients, k_L, decrease and the pore diffusion coefficients, D_{ep}, and surface diffusion coefficients, D_s, increase as SG dosages were raised from 0.5 to 4 g/L under similar initial Sb(III) concentrations. The values of k_L and D_{ep} were more dependent on initial Sb(V) concentrations rather than SG dosages, while D_s increases with increasing SG dosages. Sb(III)-loaded SG could be regenerated effectively and reused for five cycles. A 91.2% re-adsorption capacity was

retained using a 6% NaOH stripping solution. The regeneration of Sb(V)-loaded SG using NaOH solutions was not successful and needs to be improved in future work. Column performance evaluations demonstrated that Sb(III) was more successfully removed than Sb(V) prior to breakthrough (5 μg/L). The batch and column performances indicated the granular adsorbents are promising for practical application.

Supplementary material

The supplementary material for this paper is available online at [http://dx.doi.10.1080/19443994.2016.1155176].

Acknowledgments

Nomenclature

C_A	— concentration of adsorbate in aqueous solution (mg/L)
$C_{A,exp}$	— experimental concentration of adsorbate in aqueous solution (mg/L)
$C_{A,pred}$	— concentration of adsorbate in aqueous solution predicted with the PVDM or SDM model (mg/L)
C_{A0}	— concentration of adsorbate in aqueous solution (mg/L)
$C_{A,r}$	— concentration of adsorbate within the particle at distance r (mg/L)
$C_{A,r\mid r=Rp}$	— concentration of adsorbate at the external surface of the particle at r = Rp (mg/L)
C_e	— concentration of adsorbate on the equilibrium between adsrobate in solution and in solid phase (mg/L)
d_p	— average pore diameter (nm)
D_{AB}	— molecular diffusion coefficient at infinite dilution (cm^2/s)
D_{eP}	— effective pore volume diffusion coefficient (cm^2/s)
D_s	— surface diffusion coefficient (cm^2/s)
D_{s0}	— effective surface diffusion coefficient at zero surface coverage (cm^2/s)
α	— constant in Eq. (8) (g/mg)
k_L	— external mass transfer coefficient in liquid phase (cm/s)
m	— mass of adsorbent (g)
q	— mass of adsorbate adsorbed (mg/g)
q_{exp}	— experimental mass of adsorbate adsorbed (mg/g)

q_{pred}	— mass of adsorbate adsorbed predicted with the isotherm model (mg/g)
q_e	— mass of adsorbate adsorbed on the equilibrium between adsrobate in solution and in solid phase (mg/g)
C_e	— concentrations of adsorbate in solution (mg/L)
r	— radial distance (cm)
R_P	— radius of the particle (cm)
R	— universal gas constant
SA	— surface area per adsorbent mass unit (m^2/g)
S	— external surface area per mass of adsorbent (cm^2/g)
T	— temperature (K)
V	— volume of the solution (ml)

Greek symbols

ρ_P	— bulk density of the adsorbent particles (g/cm^3)
ε_P	— void fraction of the adsorbent particles

References

[1] M. Filella, N. Belzile, Y.-W. Chen, Antimony in the environment: A review focused on natural waters, Earth-Sci. Rev. 57 (2002) 125–176.

[2] F. Paoletti, P. Sirini, H. Seifert, J. Vehlow, Fate of antimony in municipal solid waste incineration, Chemosphere 42 (2001) 533–543.

[3] S.C. Wilson, P.V. Lockwood, P.M. Ashley, M. Tighe, The chemistry and behaviour of antimony in the soil environment with comparisons to arsenic: A critical review, Environ. Pollut. 158 (2010) 1169–1181.

[4] A. Pierart, M. Shahid, N. Séjalon-Delmas, C. Dumat, Antimony bioavailability: Knowledge and research perspectives for sustainable agricultures, J. Hazard. Mater. 289 (2015) 219–234.

[5] X. Guo, Z. Wu, M. He, Removal of antimony(V) and antimony(III) from drinking water by coagulation–flocculation–sedimentation (CFS), Water Res. 43 (2009) 4327–4335.

[6] H. Canada, Guidelines for Canadian drinking water quality—Summary table, Water and Air Quality Bureau, Healthy Environments and Consumer Safety Branch, Health Canada, Ottawa, Ontario, (2014).

[7] World Health Organization, Guidelines for Drinking-Water Quality, Third Edition Incorporating the First and Second Addenda, Geneva, 2008.

[8] Ministry of Health, P.R. China, Standards for drinking water quality (GB 5749-2006), (2006).

[9] X. Guo, Z. Wu, M. He, X. Meng, X. Jin, N. Qiu, J. Zhang, Adsorption of antimony onto iron oxyhydroxides: Adsorption behavior and surface structure, J. Hazard. Mater. 276 (2014) 339–345.

[10] S. Mitsunobu, Y. Takahashi, Y. Terada, M. Sakata, Antimony(V) incorporation into synthetic ferrihydrite, goethite, and natural iron oxyhydroxides, Environ. Sci. Technol. 44 (2010) 3712–3718.

[11] S. Mitsunobu, Y. Takahashi, Y. Sakai, K. Inumaru, Interaction of synthetic sulfate green rust with antimony(V), Environ. Sci. Technol. 43 (2009) 318–323.

[12] S. Dong, X. Dou, D. Mohan, C.U. Pittman Jr., J. Luo, Synthesis of graphene oxide/schwertmannite nanocomposites and their application in Sb(V) adsorption from water, Chem. Eng. J. 270 (2015) 205–214.

[13] T. Nagano, N. Yanase, Y. Hanzawa, M. Takada, H. Mitamura, T. Sato, H. Naganawa, Evaluation of the affinity of some toxic elements to schwertmannite in natural streams contaminated with acid mine drainage, Water Air Soil Pollut. 216 (2011) 153–166.

[14] A. Goswami, M.K. Purkait, Removal of fluoride from drinking water using nanomagnetite aggregated schwertmannite, J. Water Process Eng. 1 (2014) 91–100.

[15] E.D. Burton, R.T. Bush, S.G. Johnston, K.M. Watling, R.K. Hocking, L.A. Sullivan, G.K. Parker, Sorption of arsenic(V) and arsenic(III) to schwertmannite, Environ. Sci. Technol. 43 (2009) 9202–9207.

[16] X. Dou, D. Mohan, C.U. Pittman Jr., Arsenate adsorption on three types of granular schwertmannite, Water Res. 47 (2013) 2938–2948.

[17] U. Schwertmann, R.M. Cornell, Iron Oxides in the Laboratory: Preparation and Characterization, Wiley-Vch, Weinheim, 2000.

[18] Y. Liao, J. Liang, L. Zhou, Adsorptive removal of As (III) by biogenic schwertmannite from simulated As-contaminated groundwater, Chemosphere 83 (2011) 295–301.

[19] Y. Liao, L. Zhou, S. Bai, J. Liang, S. Wang, Occurrence of biogenic schwertmannite in sludge bioleaching environments and its adverse effect on solubilization of sludge-borne metals, Appl. Geochem. 24 (2009) 1739–1746.

[20] X. Dou, Y. Zhang, M. Yang, Y. Pei, X. Huang, T. Takayam, S. Kato, Occurrence of arsenic in groundwater in the suburbs of beijing and its removal using an iron-cerium bimetal oxide adsorbent, Water Qual. Res. J. Can. 41 (2006) 140–146.

[21] J.D. Méndez-Díaz, G. Prados-Joya, J. Rivera-Utrilla, R. Leyva-Ramos, M. Sánchez-Polo, M.A. Ferro-García, N.A. Medellín-Castillo, Kinetic study of the adsorption of nitroimidazole antibiotics on activated carbons in aqueous phase, J. Colloid Interface Sci. 345 (2010) 481–490.

[22] R. Ocampo-Perez, R. Leyva-Ramos, P. Alonso-Davila, J. Rivera-Utrilla, M. Sanchez-Polo, Modeling adsorption rate of pyridine onto granular activated carbon, Chem. Eng. J. 165 (2010) 133–141.

[23] R. Leyva-Ramos, C.J. Geankoplis, Diffusion in liquid-filled pores of activated carbon. I. Pore volume diffusion, Can. J. Chem. Eng. 72 (1994) 262–271.

[24] R. Ocampo-Perez, R. Leyva-Ramos, J. Mendoza-Barron, R.M. Guerrero-Coronado, Adsorption rate of phenol from aqueous solution onto organobentonite: Surface diffusion and kinetic models, J. Colloid Interface Sci. 364 (2011) 195–204.

[25] R. Leyva-Ramos, C.J. Geankoplis, Model simulation and analysis of surface diffusion of liquids in porous solids, Chem. Eng. Sci. 40 (1985) 799–807.

[26] R. Leyva-Ramos, J. Rivera-Utrilla, N.A. Medellin-Castillo, M. Sanchez-Polo, Kinetic modeling of fluoride adsorption from aqueous solution onto bone char, Chem. Eng. J. 158 (2010) 458–467.

[27] R. Ocampo-Pérez, M.M. Abdel daiem, J. Rivera-Utrilla, J.D. Méndez-Díaz, M. Sánchez-Polo, Modeling adsorption rate of organic micropollutants present in

landfill leachates onto granular activated carbon, J. Colloid Interface Sci. 385 (2012) 174–182.

[28] C.J. Radke, J.M. Prausnitz, Adsorption of organic solutes from dilute aqueous solution of activated carbon, Ind. Eng. Chem. Fundam. 11 (1972) 445–451.

[29] T. Furusawa, J.M. Smith, Fluid-particle and intraparticle mass transport rates in slurries, Ind. Eng. Chem. Fundam. 12 (1973) 197–203.

[30] G. Sewell, PDE2D: Easy-to-use software for general two-dimensional partial differential equations, Adv. Eng. Soft. 17 (1993) 105–112.

[31] J. Xi, M. He, C. Lin, Adsorption of antimony(III) and antimony(V) on bentonite: Kinetics, thermodynamics and anion competition, Microchem. J. 97 (2011) 85–91.

[32] I. Langmuir, The constitution and fundamental properties of solids and liquids, J. Am. Chem. Soc. 38 (1916) 2221–2295.

[33] H.M.F. Freundlich, Űber die adsorption in lősungen, Z. Phys. Chem. 57 (1906) 385–470.

[34] S.E. Mason, T.P. Trainor, C.J. Goffinet, DFT study of Sb(III) and Sb(V) adsorption and heterogeneous oxidation on hydrated oxide surfaces, Comput. Theor. Chem. 987 (2012) 103–114.

[35] M. He, X. Wang, F. Wu, Z. Fu, Antimony pollution in China, Sci. Total Environ. 421–422 (2012) 41–50.

[36] X. Zhao, X. Dou, D. Mohan, C.U. Pittman Jr., Y.S. Ok, X. Jin, Antimonate and antimonite adsorption by a polyvinyl alcohol-stabilized granular adsorbent containing nanoscale zero-valent iron, Chem. Eng. J. 247 (2014) 250–257.

[37] C. Shan, Z. Ma, M. Tong, Efficient removal of trace antimony(III) through adsorption by hematite modified magnetic nanoparticles, J. Hazard. Mater. 268 (2014) 229–236.

[38] X. Yang, Z. Shi, L. Liu, Adsorption of Sb(III) from aqueous solution by QFGO particles in batch and fixed-bed systems, Chem. Eng. J. 260 (2015) 444–453.

[39] R. Watkins, D. Weiss, W. Dubbin, K. Peel, B. Coles, T. Arnold, Investigations into the kinetics and thermodynamics of Sb(III) adsorption on goethite (α-FeOOH), J. Colloid Interface Sci. 303 (2006) 639–646.

[40] X. Li, X. Dou, J. Li, Antimony(V) removal from water by iron-zirconium bimetal oxide: Performance and mechanism, J. Environ. Sci. 24 (2012) 1197–1203.

[41] F. Kolbe, H. Weiss, P. Morgenstern, R. Wennrich, W. Lorenz, K. Schurk, H. Stanjek, B. Daus, Sorption of aqueous antimony and arsenic species onto akaganeite, J. Colloid Interface Sci. 357 (2011) 460–465.

[42] Y. Miao, F. Han, B. Pan, Y. Niu, G. Nie, L. Lv, Antimony(V) removal from water by hydrated ferric oxides supported by calcite sand and polymeric anion exchanger, J. Environ. Sci. 26 (2014) 307–314.

[43] K.K.H. Choy, J.F. Porter, G. McKay, Film-surface diffusion during the adsorption of acid dyes onto activated carbon, J. Chem. Technol. Biotechnol. 79 (2004) 1181–1188.

[44] R. Leyva-Ramos, L.A. Bernal-Jacome, J. Mendoza-Barron, M.M.G. Hernandez-Orta, Kinetic modeling of pentachlorophenol adsorption onto granular activated carbon, J. Taiwan Inst. Chem. Eng. 40 (2009) 622–629.

[45] A.H. Mollah, C.W. Robinson, Pentachlorophenol adsorption and desorption characteristics of granular activated carbon—I. Isotherms, Water Res. 30 (1996) 2901–2906.

[46] J. Jönsson, P. Persson, S. Sjöberg, L. Lövgren, Schwertmannite precipitated from acid mine drainage: Phase transformation, sulphate release and surface properties, Appl. Geochem. 20 (2005) 179–191.

[47] USEPA, Treatment of Arsenic Residuals from Drinking Water Removal Processes, EPA/600/R-01/033, Newport News, VA, (2001).

[48] X. Wu, Y. Zhang, X. Dou, M. Yang, Fluoride removal performance of a novel Fe–Al–Ce trimetal oxide adsorbent, Chemosphere 69 (2007) 1758–1764.